Synthesis of a multiple-peak spatial degree of coherence for imaging through absorbing media

Mark Gokhler and Joseph Rosen

The synthesis of a multiple-peak spatial degree of coherence is demonstrated. This degree of coherence enables us to scan different sample points on different altitudes simultaneously and thus decreases the acquisition time. The multipeak degree of coherence is also used for imaging through an absorbing layer with different thicknesses or different indices of refraction along the layer. All our experiments are performed with a quasi-monochromatic light source. Therefore problems of dispersion and inhomogeneous absorption are avoided. Our experimental results are presented. © 2005 Optical Society of America

OCIS codes: 120.3180, 030.1640, 030.6600, 120.6650, 070.2580, 120.2830, 120.3940.

1. Introduction

Synthesizing the degree of coherence with multiple peaks was recently proposed by Teramura *et al.*[1] They synthesized a temporal coherence function that can simultaneously scan different planes of a three-step object without any mechanical movement. We, however, propose to construct a multiple-peak spatial longitudinal degree of coherence that can also simultaneously inspect various sample points on different altitudes and thus can reduce the overall scanning time.

The longitudinal spatial degree of coherence is determined by the radial intensity distribution of a quasi-monochromatic incoherent light source according to a particular interpretation of the van Cittert–Zernike theorem.[2] In the present study we suggest synthesizing the intensity distribution of the light source to generate a multipeak spatial degree of coherence. A key element of the method is an electrically addressed spatial light modulator (SLM) that can spatially modulate the intensity distribution of the light. Using the SLM, one can get complete control of the amplitude and the phase of the degree of coherence in the system without moving any component in the profilometer.[3–5] Compared with the corresponding temporal method,[1] using a quasi-monochromatic light source eliminates the effects of dispersion that might otherwise limit the use of optical coherence tomography systems.

The multipeak degree of coherence can also be used for imaging through a scattering and absorbing media of variable thickness. Seeing through scattering media is of prime importance in biomedical imaging. Although media absorption is significant, many biological tissues have spectral windows at wavelengths of 650–1400 nm in which their absorption is less severe and scattering is the main obstruction. In many experiments with scattering there is some percentage of nonscattered light, termed ballistic light. This ballistic light forms a shadow image of any absorbing object buried in the medium. For relatively modest scattering depths there are several possible gating techniques[6] for blocking the scattering light and forming images from the ballistic light.

One of the gating techniques for catching the ballistic light, developed by Leith *et al.*,[7] uses holography with spatially incoherent illumination. An object embedded in a scattering medium is placed in one arm of an interferometer and interferes on the hologram plane with a reference beam coming from the other arm. The system is adjusted such that only the optical paths of the ballistic light and the reference beam are equal. Therefore, only the image carried by the ballistic light is recorded as a hologram, whereas all the scattered light contributes to a uniform background level. A high-dynamic range CCD is required for recording those holograms because of the intense background illumination from the scattering light.

The authors are with the Department of Electrical and Computer Engineering, Ben-Gurion University of the Negev, P.O. Box 653, Beer-Sheva 84105, Israel. J. Rosen's e-mail address is rosen@ee.bgu.ac.il.

Received 7 July 2004; revised manuscript received 19 September 2004; accepted 20 September 2004.

0003-6935/05/152921-07$15.00/0

Recently techniques with photorefractive holography[8] that are insensitive to uniform background illumination were developed. In the present study we describe an experiment of imaging through an absorbing medium of variable thickness by use of a variable gating technique. By shaping the longitudinal spatial degrees of coherence to a multipeak function we can observe various parts of the object through the medium even when they are covered with a layer of different thicknesses or different indices of refraction. In addition, by sculpturing the degree of coherence, this method enables us to see through the medium without moving any part of the interferometer. We believe that applying our method with more-sensitive equipment will enable us to see through scattering media as well.

2. Longitudinal Spatial Coherence Profilometer

The details of the longitudinal spatial coherence profilometer were reported in Refs. 3–5, and therefore they are only briefly reviewed here. A schematic illustration of the profilometer is shown in Fig. 1(a). A laser beam illuminates the SLM and images the SLM pattern through lens L_0 onto a rotated diffuser, thus creating a quasi-monochromatic incoherent source with an arbitrary shape. Light from this source propagates through lens L_1 and is split into two beams by a beam splitter. One beam is reflected from the tested surface (S), and the other is reflected from the reference mirror (R). The two reflected beams are combined and recorded by a CCD camera after they pass through lens L_2. Lens L_2 images the sample plane onto the CCD. Reference R and sample S mirrors are located at distances $z = L$ and $z = L + \Delta z$, respectively, from the rear focal point. Neglecting the tilt angles between the sample and the reference mirrors, we determine the visibility of the interference fringes versus longitudinal difference Δz between the mirrors by measuring the absolute value of the longitudinal complex degree of coherence $\mu(\Delta z)$, given by[3]

$$\mu(\Delta z) = \frac{\int\int I_s(x_s, y_s)\exp\left[j\frac{2\pi\Delta z}{\lambda f^2}(x_s^2 + y_s^2)\right]\mathrm{d}x_s\mathrm{d}y_s}{\int\int I_s(x_s, y_s)\mathrm{d}x_s\mathrm{d}y_s}, \tag{1}$$

where λ is the wavelength of light, f is the focal length of lens L_1, and $I_s(x_s, y_s)$ is the source intensity distribution projected from the SLM onto the rotated diffuser. Note that the square radial intensity distribution of incoherent source $I_s(x_s, y_s)$ determines the shape of the longitudinal complex degree of coherence.

To achieve a longitudinal degree of coherence with multiple peaks, we display on the SLM a compound Fresnel zone plate (FZP). The compound FZP comprises several angular segments, each of which has a different number of cycles. For a longitudinal degree of coherence with N peaks on each side of the Δz axis, the pattern displayed on the SLM is a binary approximation of the following expression:

$$I_s(x_s, y_s) = 1 + \sum_{n=0}^{N-1}\left[\mathrm{rect}\left(\frac{\theta - n\pi/N}{\pi/N}\right) + \mathrm{rect}\left(\frac{\theta - n\pi/N - \pi}{\pi/N}\right)\right]\cos\{\pi\gamma_n(x_s^2 + y_s^2) + \beta_n\}, \qquad \sqrt{x_s^2 + y_x^2} \le R, \tag{2}$$

where $\theta = \arctan(y_s/x_s)$, R is the maximal radius of source, and γ_n and β_n, as we shall see, are the parameters that control the amplitude and the phase, respectively, of the degree of coherence. Examples of such a compound FZP are shown in the figures de-

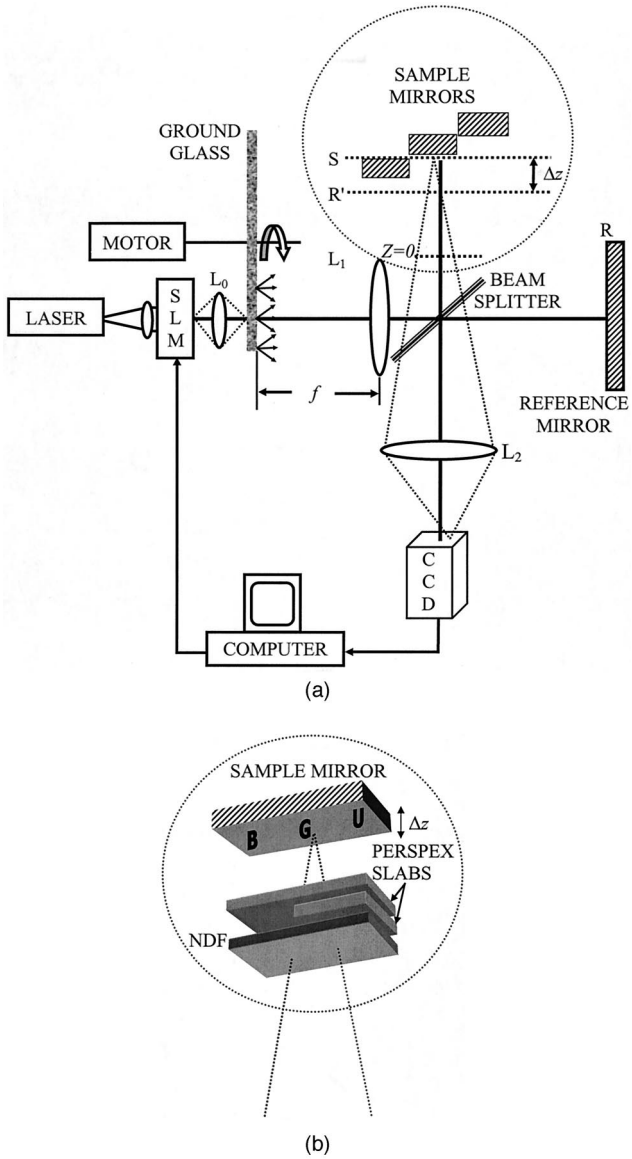

Fig. 1. (a) Schematic of the interferometric system used for the optical spatial coherence profilometry. (b) Structure of the sample arm in the system shown in (a) for the experiment of imaging through the absorbing media. NDF, neutral-density filter.

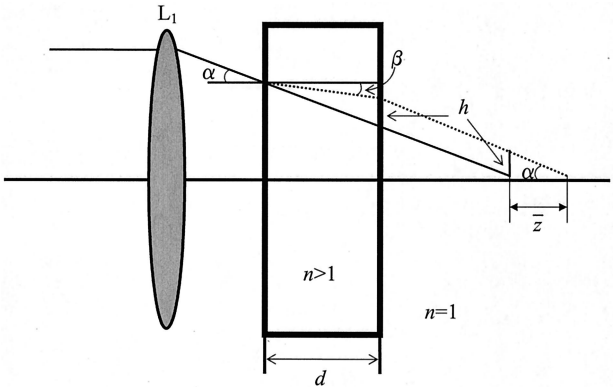

Fig. 2. Shift of the focal point of lens L_1 owing to parallel dielectric media.

scribing the experiments of this study. Substituting Eq. (2) into Eq. (1) yields the following longitudinal degree of coherence:

$$\mu(\Delta z) \propto \operatorname{sinc}\left(\frac{\Delta z R^2}{2\lambda f^2}\right) * \left[2\delta(\Delta z) + \frac{1}{N}\sum_{n=1}^{N}\exp(j\beta_n) \times \delta\left(\Delta z + \frac{\gamma_n \lambda f^2}{2}\right) + \exp(-j\beta_n)\delta\left(\Delta z - \frac{\gamma_n \lambda f^2}{2}\right)\right], \quad (3)$$

where the asterisk means convolution, δ is the Dirac delta function, and $\operatorname{sinc}(x) = \sin(\pi x)/\pi x$. Note that the compound FZP creates a complex degree of coherence with two sets of N peaks on both sides of the central zero-order peak. Each nth segment with value γ_n creates a different side peak in the coherent function, and this peak reveals a different plane on the tested sample with an altitude Δz_n above the reference plane given by

$$\Delta z_n = \gamma_n \lambda f^2/2. \quad (4)$$

According to Eq. (3), the width of each peak and thus the smallest distinguishable altitude difference is determined by the width of the sinc function, as follows:

$$\Delta z_{\min} = 2\lambda f^2/R^2. \quad (5)$$

3. Longitudinal Spatial Coherence in the Presence of a Partially Absorbing Medium

The effect of an optically thick film positioned along the light path of one of the interferometer arms was experimentally investigated by Ryabukho *et al.*[9] Their investigation is extended here, and adapted to our setup, so we may rigorously explain the effect of the additional medium in one of the arms on the longitudinal coherence function.

Introducing a uniform dielectric medium into one of the interferometer arms shifts the front focal point of lens L_1 forward along this arm relative to the focal point in the other arm. Owing to double refraction of the beam, this shift $\bar{z}$ can be evaluated in the paraxial approximation ($\tan\alpha \cong \sin\alpha$ and $\tan\beta \cong \sin\beta$) with the help of Fig. 2, as follows:

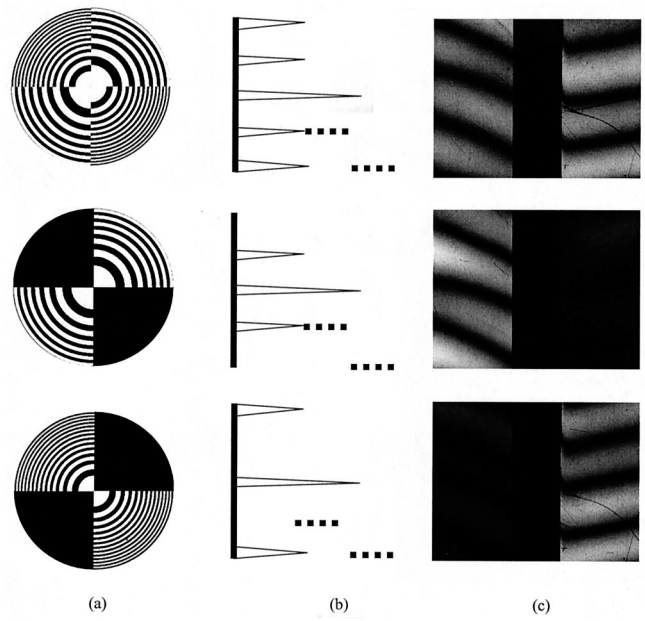

Fig. 3. (a) Set of FZPs with different values of γ_n for different angular segments. (b) Schematics of the complex degree of coherence in relation to two mirror positions. (c) Absolute values of the subtraction of two fringe images taken with β_m equal 0 and π.

$$\bar{z} = h/\tan\alpha = d(\tan\alpha - \tan\beta)/\tan\alpha = d(n-1)n, \quad (6)$$

where a trigonometric relation, $h = d(\tan\alpha - \tan\beta)$, and Snell's law, $\tan\beta/\tan\alpha \cong \sin\beta/\sin\alpha = 1/n$, are used.

We start our analysis by observing the complex amplitude behind a spherical lens. This complex amplitude is created from a single point source with complex amplitude $u_s(x_s, y_s)$ located on the front focal plane and is given by[2]

$$u(x, y, z) = \frac{u_s(x_s, y_s)}{j\lambda f}\exp\left[j\frac{2\pi(z+2f)}{\lambda} - j\frac{2\pi}{\lambda f} \times (x_s x + y_s y) + j\frac{\pi z}{\lambda f^2}(x_s^2 + y_s^2)\right], \quad (7)$$

where (x, y, z) are the coordinates behind the lens with their origin at the rear focal point. The first term in the exponent stands for the overall optical path, (the lens's thickness is neglected). The third term is actually an expression of the McCutchen theorem,[10] which expresses that each point source induces a Fourier harmonic along the z axis with a frequency related to the square of the radius of the source point at (x_s, y_s). It is important to note that the origin of this Fourier axis is at the rear focal point. When we shift this focal point without changing the system's focal distance, the Fourier distribution is also shifted accordingly.

Returning to the interferometer of Fig. 1, we indicate distance L as the distance between the rear focal point at the reference arm ($z = 0$) and the detection plane, and we assume that this optical path is constant. At the reference arm the space between the lens and the mirror is free of any obstacle, and therefore a single point from the entire source, at some point (x_s, y_s), induces behind the lens at $z = L$ a complex amplitude that is identical to the expression given in Eq. (7).

In the sample arm, where the dielectric medium with thickness d and index of refraction n is positioned between the lens and the reflecting surface, the focal point is shifted forward a distance $\bar{z}$ in each pass of the light, overall $2\bar{z}$ beyond the original focal point. In addition, the sample plane is free to move back and forth a distance Δz more, or less, than the reference arm. The effect on the complex amplitude behind the lens is expressed differently in the two phase terms of Eq. (7). Because of the interferometer's structure, the optical path is $2\Delta z$ longer than in the reference arm. On the one hand, the optical path increases by $2\Delta z + 2d(n - 1)$ owing to the shift of the sample plane and to the propagation of light in the medium with a higher index of refraction. But, on the other hand, the origin of the longitudinal Fourier axis is shifted forward by a distance $2\bar{z}$. Therefore the complex amplitude distribution in the sample arm, a distance $L + 2\Delta z$ from the original, nonshifted, rear focal point, as a result of a source point at (x_s, y_s) is

$$u_S(x, y, L + \Delta z) = \frac{u_s(x_x, y_s)}{j\lambda f} \times \exp\left[j2\pi \frac{L + 2\Delta z + 2d(n-1) + 2f}{\lambda} - j\frac{2\lambda}{\lambda f}(x_s x + y_s y) + j\frac{\pi(L + 2\Delta z - 2\bar{z})}{\lambda f^2}(x_s^2 + y_s^2)\right]. \quad (8)$$

Note that, although the optical path is increased owing to the presence of an additional optical path through the dielectric medium as expressed in the first term of the exponent, the longitudinal Fourier axis is shortened by $2\bar{z}$ because of the shift of the focal point, as expressed in the third term of the exponent. As we shall see next, this phenomenon causes the spatial longitudinal coherence function to shift in the direction opposite that of the temporal coherence function, although both functions are shifted because of the same dielectric medium.[9]

The two complex amplitudes at the sample and the reference arms, which originated from the same source point, interfere coherently. However, the contributions from all other source points are summed incoherently because of the incoherent nature of the source. When the sample surface is tilted by a small angle (φ_x, φ_y) relative to the transverse plane, the direction of the reflected beam deviates by an angle $(2\varphi_x, 2\varphi_y)$ from its original direction. This introduction of angular deviation is equivalent to giving lateral displacement $(\Delta x, \Delta y) = [f\tan(2\varphi_x), f\tan(2\varphi_y)]$ to the point source observed from the sample arm. As each point source is completely incoherent to any other points on the source, the overall intensity on the image sensor contributed from all the source points is a sum of fringe intensities obtained from each point source[5]:

$$I(x, y, L) = \int |u_s(x, y, L + 2\Delta z) + u(x, y, L)|^2 dx_s dy_s = A\left(1 + |\mu(\Delta x, \Delta y, \Delta z)|\cos\left\{\frac{2\pi}{\lambda f}(x\Delta x + y\Delta y) + \frac{4\pi[\Delta z + d(n-1)]}{\lambda} + \phi(\Delta x, \Delta y, 2\Delta z) + \frac{\pi(L + 2\Delta z - 2\bar{z})}{\lambda f^2} \times (\Delta x^2 + \Delta y^2)\right\}\right), \quad (9)$$

where A is a constant and function $\mu(\Delta x, \Delta y, 2\Delta z) = |\mu(\Delta x, \Delta y, 2\Delta z)|\exp[j\phi(\Delta x, \Delta y, 2\Delta z]$ is the three-dimensional complex degree of coherence given by[2]

$$\mu(\Delta z, \Delta x, \Delta y) = \frac{1}{\iint I_s(x_s, y_s)dx_s dy_s} \times \iint I_s(x_s, y_s)\exp\left[j\frac{2\pi(\Delta z - \bar{z})}{\lambda f^2} \times (x_s^2 + y_s^2) - j\frac{2\pi(L + 2\Delta z - 2\bar{z})}{\lambda f^2} \times (x_s\Delta x + y_s\Delta y)\right]dx_s dy_s. \quad (10)$$

For a small and constant tilt angle of the sample mirror and therefore small and constant values of $(\Delta x, \Delta y)$, the three-dimensional degree of coherence can be approximated to a longitudinal degree of coherence as follows:

$$\mu(\Delta z) = \frac{1}{\iint I_s(x_s, y_s)dx_s dy_s} \times \iint I_s(x_s, y_s)\exp\left[j\frac{2\pi(\Delta z - \bar{z})}{\lambda f^2} \times (x_s^2 + y_s^2)\right]dx_s dy_s. \quad (11)$$

As a result of the dielectric medium, the degree of coherence is shifted to the right of the Δz axis. This means that one needs to increase the optical path of the sample arm by the value $\Delta z = \bar{z}$ to get maximum fringe visibility. This is in opposite the case of temporal coherence, for which to get maximum fringe visibility one should shorten the optical path by the value $\Delta z = d(n - 1)$ to compensate for the additional optical path inside the medium.

Using multiple peaks, one can use a longitudinal degree of coherence to observe a pattern hidden behind a dielectric layer with nonuniform thickness or with different indices of refraction. According to Eq. (11), each part of the layer shifts its degree of coherence differently, according to its thickness (or its index of refraction). If one adjusts distance Δz such that the coherence between the two arms is always on one of the coherence function peaks but a different peak for a different thickness (or for different indices of refraction), then the high fringe visibility is maintained along all the layer area. Thus the pattern behind the layer is revealed, although the optical path is different above different parts of the pattern. An example of such a situation is demonstrated in the end of Section 4 below.

4. Experimental Results

Experiments were conducted to demonstrate the validity of the theory described above. In the first experiment the compound FZP was divided into four equal segments with two values of γ: $\gamma_{1,2} = 6$, 12 cm^{-2}. The radius of the incoherent source was $R = 1.5$ cm. According to Eq. (4), the compound FZP can reveal two altitudes, $\Delta z_{1,2} \approx 425{,}850$ μm, simultaneously above the reference plane. According to Eq. (5), the minimal resolvable altitude is $\Delta z_{\min} = 126$ μm. Two flat mirrors were used as samples in this preliminary experiment. The focal lengths of lenses L_1 and L_2 were both $f = 150$ mm. Three measurements were performed with the compound FZPs shown in Fig. 3(a). To improve the contrast of the fringe patterns and to reduce the noise on the fringes we always subtract two interference patterns, one taken with a FZP phase of $\beta = 0$; the other, with $\beta = \pi$. This noise-immunity procedure is done in each measurements point Δz and for all the experiments with high orders of coherence in this study. By this procedure the fringes visibility is significantly increased and fringes caused by the zero coherence order are eliminated.[5] This is so because, according to relation (3), the phase of the zero coherence order is not influenced by the value of β. The degrees of coherence relative to the various altitudes of the two mirrors are shown in Fig. 3(b). As shown in Fig. 3(c), when a segment with γ_n reveals an altitude of a certain mirror, high fringe visibility is clearly seen on the mirror's image. Table 1 lists the visibilities on the mirror images obtained by interference subtraction for each state of the source mask.

A similar experiment, but with three mirrors and with a compound FZP of three values of γ, is described next. This time the radius of the incoherent source was $R = 2.5$ cm, and the compound FZP is displayed with three values of γ: $\gamma_{1,2,3} = 6$, 13, 21 cm^{-2}. With this compound FZP, three altitudes, $\Delta z_{1,2,3} = 425$, 920, 1487 μm, are simultaneously revealed. According to Eq. (5) the minimum resolvable altitude is 45 μm. The results of this experiment are shown in Fig. 4, whereas the visibility values of the fringes on the various mirror planes are summarized in Table 2. Comparing the results in Tables 1 and 2, we can conclude that the signal-to-noise ratio is worse in the case of three segments.

Table 1. Fringe Visibilities Measured in the Experiment with Two Sample Mirrors

Number of Segments; Value of γ	Visibility on Mirror 1	Visibility on Mirror 2
Two segments; $\gamma_{1,2} = 6$, 12 cm^{-2}	0.78	0.94
One segment; $\gamma_1 = 6$ cm^{-2}	0.81	0.41
One segment; $\gamma_2 = 12$ cm^{-2}	0.48	0.86

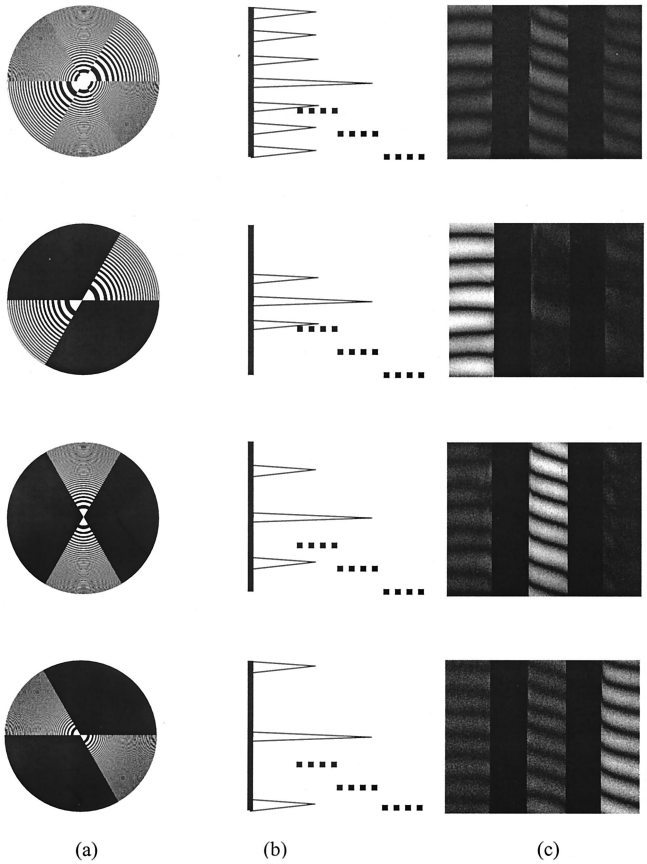

Fig. 4. (a) Set of FZPs with different values of γ_n for different angular segments. (b) Schematics of the complex degree of coherence in relation to three mirror positions. (c) Absolute value of the subtraction between two fringe images taken with β_m equal 0 and π.

Table 2. Fringe Visibilities Measured in the Experiment with Three Sample Mirrors

Number of Segments; Value of γ	Visibility on Mirror 1	Visibility on Mirror 2	Visibility on Mirror 3
Three segments; $\gamma_{1,2,3} = 6, 13, 21\ \mathrm{cm}^{-2}$	0.77	0.69	0.76
One segment; $\gamma_1 = 6\ \mathrm{cm}^{-2}$	0.96	0.21	0.24
One segment; $\gamma_2 = 13\ \mathrm{cm}^{-2}$	0.57	0.82	0.44
One segment; $\gamma_3 = 21\ \mathrm{cm}^{-2}$	0.48	0.64	0.83

This is reasonable because each segment of the three occupies only an angular section of 120° and therefore induces a lower coherence order than for two segments.

The next experiments demonstrate our method of imaging through absorbing media. First we checked the behavior of the degree of coherence when the parallel window of a glass was introduced into one arm of the interferometer to validate Eq. (6). Before introducing the dielectric medium, we calibrated the path difference between the two arms of the interferometer to equal optical paths. The focal length of lens L_1 was 35 cm. A circular disk of 2.5-cm radius was used as the incoherent source, such that the complex degree of coherence contained only the zero order. Under these conditions, and with equal paths of the two arms, a high-visibility interference pattern was observed by the CCD. Then a parallel window made from glass (Newport BK7; $n = 1.51$) with a thickness of 6 mm was inserted between the sample mirror and the beam splitter. To recover the high-visibility fringes we shifted the sample mirror a distance 2 mm away from the beam splitter. In other words, the optical path of the arm with the glass was increased to be highly coherent with the reference beam. The additional mirror shift coincides with a value obtained from Eq. (6). A similar experiment was repeated with a FZP of $\gamma = 6\ \mathrm{cm}^{-2}$ to validate the expected behavior of the first coherence order as well. When the glass was introduced into the sample arm, the same mirror shift of 2 mm away from the beam splitter was needed to reveal once more the fringes caused by the first coherence order.

Finally, experiments of imaging through absorbing media by using the effects of longitudinal spatial coherence are described. The same circular disk of 2.5-cm radius was used as the incoherent source, creating a complex degree of coherence of zero order only. Three letters, B, G, and U, were drawn on the sample mirror. Perspex slabs 5 and 10 mm thick were introduced above the letter B and above the letter U, respectively. In addition, a 2-mm-thick neutral-density filter (NDF) used as a light absorber was introduced above all the letters. This setup is depicted in Fig. 1(b), and in the interferometer it replaces the structure that appears inside the dotted circle in Fig. 1(a). After an image hologram of the sample was recorded on the CCD, the hologram was reconstructed in the computer by filtering of the information carried by the holographic grating. To obtain high fringe visibility in the vicinity of the letter B we shifted the sample mirror away from the beam splitter a distance $d_1(n - 1)/n = 2.3$ mm, where $d_1 = d_{1,\mathrm{SLAB}} + d_{\mathrm{NDF}} = 7$ mm and $n \approx 1.5$ is the refractive index of the Perspex slab and the NDF. The hologram recorded by the CCD and the results of reconstruction are shown in Figs. 5(a) and 5(b), respectively. Apparently, only the image of the letter B was revealed, because only its area was in high spatial coherence with the reference mirror. The additional optical path above the other letters reduces the degree of coherence between the arms such that the letters G and U are filtered out from the final image.

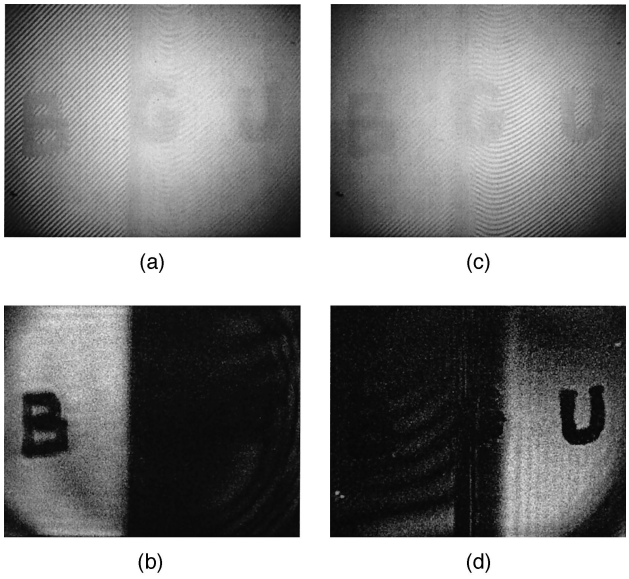

Fig. 5. (a) Image hologram recorded by the CCD when the path difference between reference and sample mirrors was $\Delta z = 2.3$ mm. (b) Digitally reconstructed image from the hologram shown in (a). (c) Image hologram recorded by the CCD when the path difference between reference and sample mirrors was $\Delta z = 4$ mm. (d) Digitally reconstructed image from the hologram shown in (c).

To obtain high fringe visibility in the vicinity of the letter U we shifted the sample mirror away from the beam splitter to distance $d_2(n - 1)/n = 4$ mm, where $d_2 = d_{2,\mathrm{SLAB}} + d_{\mathrm{NDF}} = 12$ mm. The hologram recorded by the CCD and the reconstruction results are shown in Figs. 5(c) and 5(d), respectively. Only the image of the letter U was revealed in Fig. 5(c), because only its area was in high spatial coherence with the reference mirror. The letter G was exactly under the interface between the two slabs, and therefore no hologram was recorded on its region. The shorter optical path above the letter B reduces the degree of coherence between the arms such that B is filtered out from the final image.

Using other coherence orders rather than only the zero order can yield the same results without the shifting of any mirror. Moreover, by using a com-

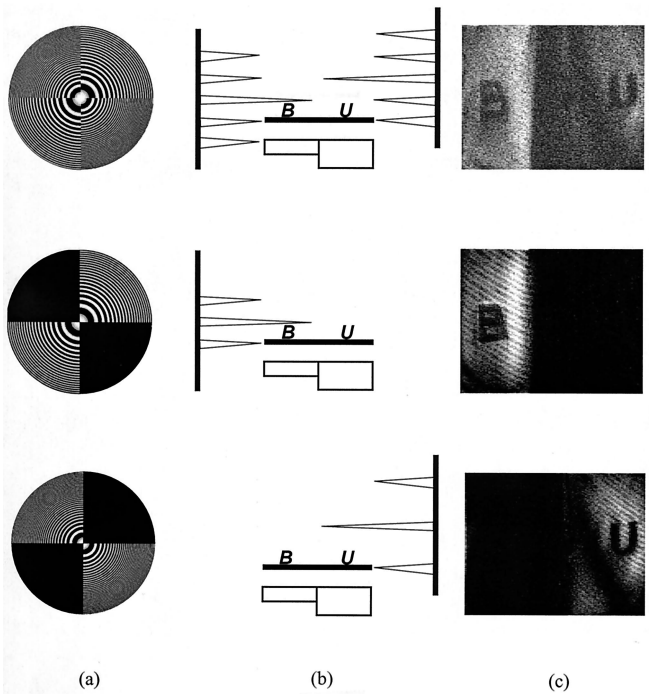

Fig. 6. (a) Set of FZP's with different values of γ_n for different angular segments. (b) Schematics of the complex degree of coherence in relation to the structure of the sample mirror covered by absorbing media. (c) Images reconstructed digitally from the holograms recorded by the CCD when the interferometer was illuminated by the FZPs shown in (a).

pound FZP, one can simultaneously reveal several letters, as demonstrated next. In contrast to the previous experiment, here the letters are exposed because of coherence matching with higher-than-zero coherence orders. A compound FZP shown in Fig. 6(a) of four segments with two values of γ_n: $\gamma_{1,2} = 6$, 10.7 cm^{-2}, is used here as the incoherent source. The radius of the incoherent source was 350 mm, and the focal length of lens L_1 was 350 mm. The FZPs create first-order peaks on distances of $\Delta z_{1,2} = 2.3$, 4.1 mm from both sides of the zero order. The smallest distinguishable altitude difference was $\Delta z = 247$ μm. Two Perspex slabs with thicknesses of 5 and 10 cm, and a 2-mm-thick NDF that transmits 25% of light intensity, were used in this experiment. Three configurations with three FZPs shown in Fig. 6(a) were tested. In each experiment FZPs with phases 0 and π were used for recording two holograms and, as before, subtraction techniques was used for creating more-efficient holograms. Reconstruction of the holograms was made by digital filtering of the information carried on the holographic grating. Positions of high-coherence-order peaks relative to the sample mirror in each experiment are shown schematically in Fig. 6(b). Finally, the images reconstructed from the holograms obtained in the three experiments are shown in Fig. 6(c). This experiment emphasizes the flexibility of using high coherence orders. By tuning only the cycle numbers of the FZP, one can observe different parts of the image, as demonstrated in the middle and bottom parts of Fig. 6. By using the compound FZP one can observe more parts of the image simultaneously, as demonstrated at the top of Fig. 6.

5. Conclusions

Synthesis of a multipeak spatial degree of coherence has been demonstrated. An analysis based on interference between couples of source points explained the main effects of the interferometric system. A series of different experiments proved the validity of the analysis. A new method of imaging through absorbing media without any mechanical movement has been presented. This method is flexible in the sense that different parts of the sample can be viewed separately or simultaneously according to the chosen shape of the coherence function and the thickness profile (or the index of refraction) of the layer covering the sample. The method can potentially be used for imaging through turbid media. All these benefits come with the advantage of working with quasi-monochromatic light such that dispersion effects are inherently avoided.

This research was supported by Israel Science Foundation grant 119/03.

References

1. Y. Teramura, K. Suzuki, M. Suzuki, and F. Kannari, "Low coherence interferometry with synthesis of coherence function," Appl. Opt. **38,** 5974–5980 (1999).
2. J. Rosen and A. Yariv, "General theorem of spatial coherence: application to three-dimensional imaging," J. Opt. Soc. Am. A **13,** 2091–2095 (1996).
3. J. Rosen and M. Takeda, "Longitudinal spatial coherence applied for surface profilometry," Appl. Opt. **39,** 4107–4111 (2000).
4. W. Wang, H. Kozaki, J. Rosen, and M. Takeda, "Synthesis of longitudinal coherence functions by spatial modulation of an extended light source: a new interpretation and experimental verifications," Appl. Opt. **41,** 1962–1971 (2002).
5. M. Gokhler, Z. Duan, J. Rosen, and M. Takeda, "Spatial coherence radar applied for tilted surface profilometry," Opt. Eng. **42,** 830–836 (2003).
6. C. Dunsby and P. M. W. French, "Techniques for depth-resolved imaging through turbid media including coherence-gated imaging," J. Phys. D **36,** R207–R227 (2003).
7. E. N. Leith, C. Chen, Y. Chen, J. Lopez, P.-C. Sun, and D. Dilworth, "Imaging through scattering media using spatial incoherence techniques," Opt. Lett. **16,** 1820–1822 (1991).
8. C. Dunsby, Y. Gu, Z. Ansari, P. M. W. French, L. Peng, P. Yu, M. R. Meloch, and D. D. Nolte, "High-speed depth-sectioned wide-field imaging using low-coherence photorefractive holographic microscopy," Opt. Commun. **219,** 87–99 (2003).
9. V. P. Ryabukho, D. V. Lyakin, and M. I. Lobachev, "The effects of temporal and longitudinal spatial coherence in a disbalanced-arm interferometer," Tech. Phys. Lett. **30,** 64–67 (2004).
10. C. W. McCutchen, "Generalized aperture and the three-dimensional diffraction image," J. Opt. Soc. Am. **54,** 240–244 (1964).